LAWRENCE
LIVERMORE
NATIONAL
LABORATORY

UCRL-PROC-233023

New experimental capabilities and theoretical insights of high pressure compression waves

D. Orlikowski, J. Nguyen, J. R. Patterson, R. Minich, L. P. Martin, N. Holmes

July 24, 2007

Shock Compression of Condensed Matter
Hilo, HI, United States
June 25, 2007 through June 29, 2007

Disclaimer

New experimental capabilities and theoretical insights of high pressure compression waves

Daniel Orlikowski*, Jeffrey H. Nguyen*, J. Reed Patterson*, Roger Minich*, L. Peter Martin* and Neil C. Holmes*

**Lawrence Livermore National Laboratory (LLNL), P.O. Box 808, L-45, Livermore, CA 94551-0808*

Abstract. Currently there are three platforms that offer quasi-isentropic compression or ramp-wave compression (RWC): light-gas gun, magnetic flux (Z-pinch), and laser. We focus here on the light-gas gun technique and on some current theoretical insights from experimental data. A gradient impedance through the length of the impactor provides the pressure pulse upon impactor to the subject material. Applications and results are given concerning high-pressure strength and liquid to solid, phase transition of water plus its associated phase fraction history. We also introduce the Korteweg-deVries-Burgers equation as a means to understand the evolution these RWC waves that propagate through the thickness of the subject material. This equation has the necessary competition between non-linear, dispersion, and dissipation processes, which is shown through observed structures that are manifested in the experimental particle velocity histories. Such methodology points towards a possible quantifiable dissipation, through which RWC experiments may be analyzed.

Keywords: Isentropic compression, wave evolution, light-gas gun, Korteweg-de Vries, solitary waves, high pressure, thermodynamics, yield strength, phase transitions

PACS: 07.35.+k,62.60.+p,05.45.Yv,64.70.Dv,62.20.Fe

INTRODUCTION

The fruition of three primary platforms (light-gas gun[1], magnetic-flux[2], and laser[3]) to apply high pressure ramp impulses to subject materials has dawned and promises to lead us to new discoveries and to help our understanding of material response at pressures approaching our sun's interior[4]. The initial efforts of ramp-wave compression(RWC) have their origin in World War II and was made more public in the 1960's (see Fowler[5]); however, not until 1970 did the first magnetic-flux experiments on hydrogen take place obtaining ~ 2 Mbar, albeit these experiments lacked support material knowledge and adequate diagnostics[6]. Though these RWC techniques are quite developed, there are many outstanding questions originally posed by Rice, McQueen, and Walsh[7] about shock wave stability that can be applied to RWC, and such interpretations are still very relevant today[8]. The questions that we pose are: Are these RWC quasi-isentropic and can that be quantified?

In this paper we focus on RWC for the light-gas gun that has been developed at LLNL, though the technology is transferrable to other platforms. Additionally, we introduce a possible quantifiable methodology of entropy production or a constraint there upon. RWC using light-gas guns with ramped impedance impactors had originated with Barker and Chhabildas[9, 10], where sedimentation of various powders was used to create an impedance gradient through the longitudinal direction of the impactor. Previous to this, fused-silica[11] and encasing, high-impedance anvils[12] could be used to perform ramp-wave compression.

Currently, the aforementioned techniques offer differing and complementary applied impulse times for their respective ramp-wave compression: through

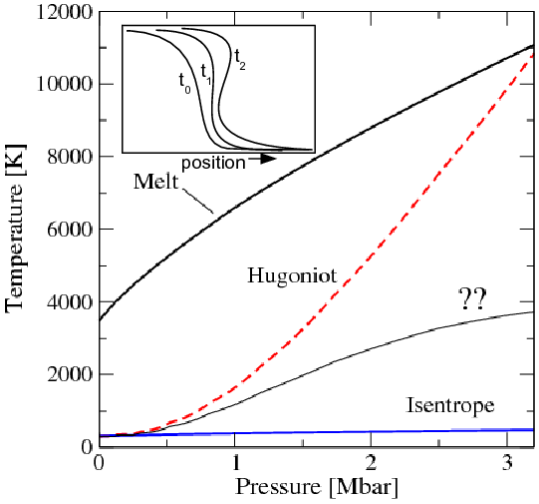

FIGURE 1. Non-linear waves t_0 eventually evolve into shock waves t_2 (inset), which means that the material at differing positions experiences differing thermodynamic paths to the peak of the wave—somewhere between the isentrope (blue-solid line) and the Hugoniot (red-dashed-line).

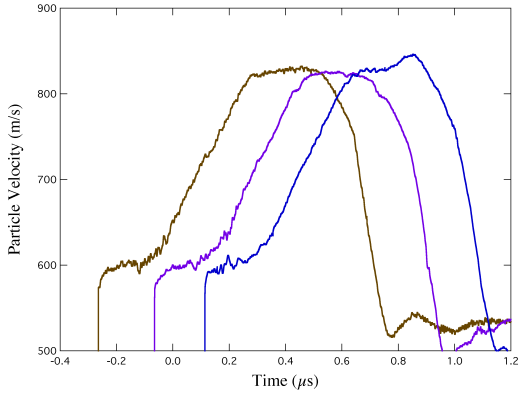

FIGURE 2. The particle velocity histories for a hot-isentrope (shock and compress) experiment on Al 1100 (thicknesses 1.5, 2.0, and 2.5 mm from left to right) using PDV[18]. The 2.5 mm is limited in time-of-experiment near 0.8 μs.

reservoir ablation onto the subject material, the laser RWC is $5-30$ ns, the magnetic flux driven RWC is $100-300$ ns, and the light-gas gun RWC is $\approx$ 2 μs. Each of these platforms have evolving technology, so the applied impulses are increasing in each case[13, 14]. It is precisely the orders of magnitude in impulse time in conjunction with dynamic diamond anvil compression (Dyn-DAC)[15] that will offer us the greatest insight into high-pressure material response (e.g. strain-rate, temperature, and kinetics effects). The caveat that needs to be mentioned here is that in these RWC experiments the wave launched into the material is evolving and taking the subject material from some initial material state $\mathscr{S}_0$ through a sequence of states to some peak or final state $\mathscr{S}_n$ with a possible following rarefaction wave or any combination of that (Fig. 1). Therefore, to really determine and eventually model the response of the material, requires temperature and phase or structure information throughout its RWC history, some of which is being developed(see articles in this proceedings and others specifically pyrometry[16] and x-ray diffraction[17]).

This paper is one of three complementary papers in this proceedings—each paper specific to the three RWC techniques. In the first section, we discuss current light-gas gun RWC impactor technology recently developed at Lawrence Livermore National Laboratory (LLNL) and its latest applications. The second section introduces very recent insights into high-pressure wave evolution through the well established Korteweg-deVries-Burgers equation. And finally we conclude with a general discussion.

LIGHT-GAS GUN ARBITRARY APPLIED IMPULSES

The light-gas gun impactor technology developed recently actually offers more than just RWC. The impactor can be designed to apply any combination of ramp compression, shock compression, and rarefaction to a system allowing for a variety of material responses to be studied from standard and elevated temperature isentropes to kinetics of phase transformations or to even hysteresis in material response[1].

For the simplest monotonic RWC, the impactor consists of a monotonic, gradient of acoustic impedance in the longitudinal direction. The impactors are composed of approximately $20-30$ μm layers; each of a specific acoustic impedance $Z(T,\rho)=\rho c$ for density ρ and sound speed $c(T,\rho)$, and as a composite it is often referred to as gra-

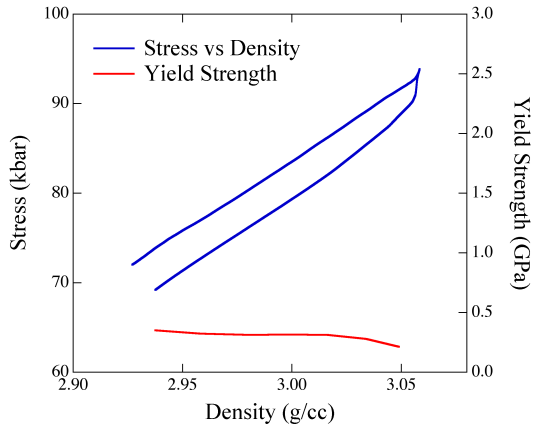

FIGURE 3. The stress as a function of density from the particle velocity histories (Fig. 2) as calculated from Lagrangian analysis is shown (upper blue curve and left axis). The yield as calculated from the difference between the compression and release is also given over the range (lower red curve and right axis). The strain-rate is nearly equal in compression as in release.

dient density impactor (GDI) or as functionally gradient material (FGM) impactor. Non-destructive and destructive characterization of the impactors have been performed and are also used to ensure on-going quality of manufacturing. The main technique currently used is that of tape-casting, which is organic-binded metal powder (Mg and Cu) sheets—each of specific metal percentage—cut, baked, and hot-pressed together to create the prescribed impedance profile. The porosity, determined from measured versus calculated densities, optical, and SEM scans, is extremely low ($<$1.5%) in the bulk of the finished impactor, with a slight increase to $\sim$ 4% in the highest-density, single-composition layer. Repeated measurements of obtained densities, sound velocities, and impedances for these layers are within 1% of predicted properties. Also, ultrasonic C-scan (acoustic time of flight) measurements indicate the entire impactor adheres to a uniform planarity as well as bulk composition standards across the impactor of $<$ 2%[19, 20, 21].

Reproducibility from shot-to-shot can be also affected by the tilt of the impactor onto the subject material for light-gas gun experiments. This is systematically managed through either an array of timing-pins (for initially shocked cases) or of PDV probes[18] (for standard RWC cases). Moreover, in general each light-gas gun has characterized tilt. Both aspects in conjunction diminish systematically the tilt error to $<$1% corresponding to a few ps in time across the impact plane.

Additionally, absolute timing is accomplished through two different methods depending upon the characteristics of the experiment. With a window material, e.g. LiF, in parallel to the subject material, PDV or VISAR[22] probes record the time of impact at the impact surface, which are synchronized to similar particle velocity records from the back surface of the subject material. This can be used either for experiments of the standard isentrope or for experiments consisting of a shock followed by compression.

With this FGM impactor a variety of experiments provide the necessary tools to aid in our understanding of high-pressure material response. Moreover, due to the simplicity of the mechanics of the experiment (i.e. a mass impacting another mass), the possibility to leverage the hydrodynamic codes to simulate the *entire* experiment allows theorists and designers benchmarks for equation-of-state (EOS) and constitutive material models, which may include 1- and 2-dimensional rarefaction waves. These types of experiments have been performed specifically for copper, where simple and/or complex thermodynamic paths were carried out through similar simple and/or complex impactor impedance profiles: standard ramp compression, shock and ramp compress, shock, release, and ramp compress, or any combination thereof[1]. However, that work was with rudimentary impactors, and now the FGM impactor has been improved upon by the aforementioned methodology and fabrication process.

Currently, the focus of FGM light-gas gun experiments has been along elevated temperature or *hot* isentropes, where the subject material or system is initially shocked completely and then ramp-compressed obtaining material states away from both the standard Hugoniot and the standard isentrope. Here the investigations are two fold: the EOS is being measured, meaning the total longitudinal stress and density can be extracted from the particle velocity U_p histories and subsequently the yield strength is extracted, where the system undergoes an additional 1-D designed rarefaction.

The methodology of extracting an EOS from U_p has been widely studied(see for example[23, 24, 25, 26, 27]). However, interpretation of U_p becomes

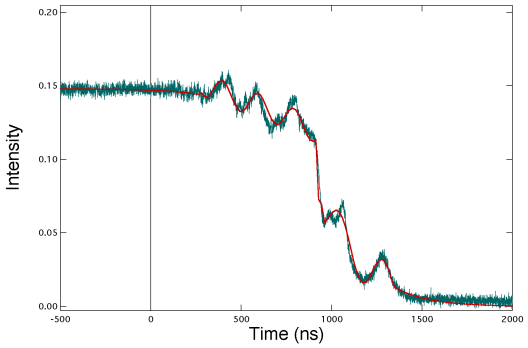

FIGURE 4. The measured ellipsometry intensity at the interface of iron sample and water as a function of time. The onset of compression is at $t = 0$. The birefringence indicates the onset of crystallization of the water near the interface. The smooth line is a running average that was performed on the original data to reduce some noise for Fig. 5.

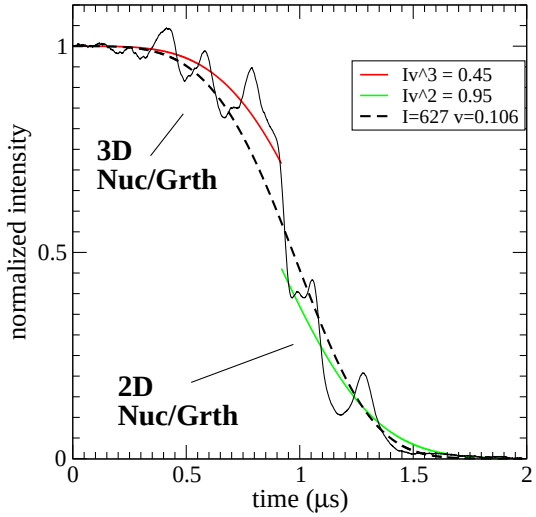

FIGURE 5. The normalized intensity (I/I_0) from Fig. 4 is given with fits using Eqn. 1 for the phase fraction history. The phase fraction model suggests that there is initially a 3-D followed by 2-D growth process of the crystallites.

difficult when strength is included into the analysis, leading to several, backward-calculated, applied pressure ramps for the same measured U_p[26]. Alternative methods of analysis are possible that attempt to account for dissipation in the system as well, but this requires knowledge of the 3^{rd} order elastic moduli[28, 29, 30]. With this in mind and within the von Mises yield criterion, the yield strength at pressure and temperature can be extracted[31, 32]. In Fig. 3 three Al 1100 samples(1.5, 2.0, and 2.5 mm thick) were first initially shocked, so that each sample starts from the same Hugoniot locus point, and then ramp compressed and released. The stress and yield are related thusly, $\sigma = P \pm \frac{2}{3}Y$ at pressure P (plus for compression and minus for release). Therefore, the difference between compression and release is $\frac{4}{3}Y$. This gives $Y \approx 0.4\ GPa$ at $P \approx 7-13\ GPa$ which is consistent with previous work[31, 32]. An important point here is that strain-rate $\dot{\varepsilon}$ is similar in loading/unloading reducing possible strain-rate effects. It should be mentioned that σ really contains some component of work hardening, since the system is not perfectly plastic.

Another experiment to pressure-induce a liquid-ice transition for water along an isentrope at approximately 2 GPa was performed that uses ellipsometry[] to record the transition at the leading edge of a very thick water sample (10 mm), thus avoiding any complications of wave reverberation or nucleation on the back interface. In Fig. 4 the ellipsometry record contains a birefringence signal after $\approx 250\ ns$ indicating the onset of an optically anisotropic crystalline structure forming in the water at the reflection surface. Moreover, the intensity record from the same experiment can be interpreted as a phase fraction over a volume element, which has a longitudinal thickness between the optical thickness and thickness of the mixed region. The phase fraction as function of growth velocity v and time t with d-dimensional constant a_d and an offset time t_0 has the form:[33, 34, 35, 36]

$$X = 1 - exp\left[\frac{a_d}{d+1} I v^d (t-t_0)^{d+1}\right] \qquad (1)$$

where the nucleation rate I is related to the Gibbs free energy difference between phases at temperature T with an initial nucleation rate of I_0

$$I = I_0\, exp(-\Delta G/k_B T)\,. \qquad (2)$$

From fitting this form and assuming that $v = 0.11 cm/\mu s$ determined from previous (not shown) multi-thickness experiments and setting t_0 to zero, gives $I = 627(\mu s cm)^{-1}$ for d = 3 (Fig. 5). Also, performing the fits in a piecewise manner, for d=3 then d=2, better fits are obtained as indicated, suggesting that the leading nucleation would be 3-D

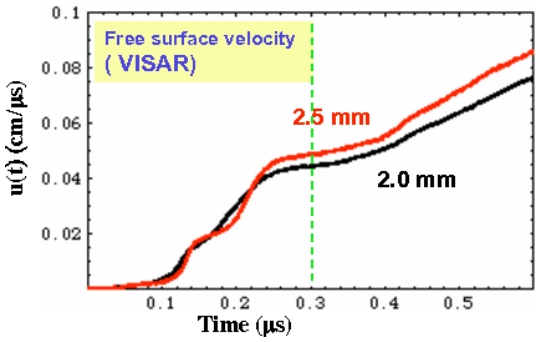

FIGURE 6. Typical Up history from two sample thicknesses(2 and 2.5 mm) shifted in time to have the same initial time.

in nature and then transitions to a 2-D growth later in time.

Two other types of experiments, in which the FGM impactor is currently being employed, is only briefly mentioned here—experiments that contribute to our understanding of material response: shear wave measurements and recovery experiments. The shear wave measurement are in collaboration with Florando *et al.*[37] and are just producing results. Recently however, recovery experiments of monocrystalline copper were performed, where the light-gas gun RWC was allowed to evolve into a shock in a 5 mm thick sample and is compared to shock compressed copper via laser drive. The main observation is that in the RWC case there is a higher pressure for the onset of stacking faults and twinning is required[38]. Also, this suggests the material response is dependent upon the path to the final state, i.e. in the RWC lower strain-rates and temperatures contribute to observed differences in the recovered material state.

UBIQUITOUSLY OBSERVED WAVE STRUCTURES

We present here very recent observations that span the three RWC drive platforms: light-gas gun[1], magnetic flux[2], and laser[3]. However, first lets state the obvious in that RWC is inherently nonlinear due to the sound speed depending upon the density and therefore causing the high-pressure states in the compression wave to travel faster than

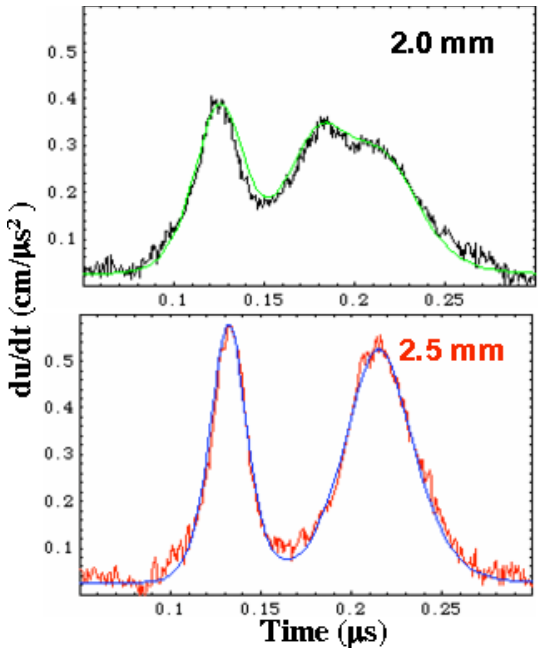

FIGURE 7. The acceleration profile $\Gamma(t)$ for the 2 mm (top) and 2.5 m (bottom) thicknesses Fig. 6 with fitting a series of $sech^2(\cdot)$-functions given in the text.

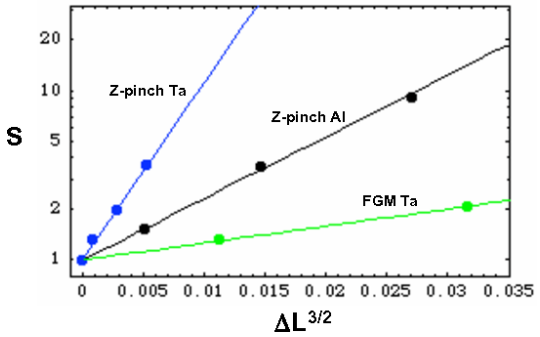

FIGURE 8. The scaled amplitudes $S = A(t)/A(0)$ as a function of position x, that have the functional form $S = exp[\lambda_0 \kappa^2 \Delta L^{3/2}]$. The points are from RWC experiments: tantalum Z-pinch[39], aluminum Z-pinch[14], and tantalum GDI[40].

the low-pressure states leading eventually to shock formation. This wave evolution in these RWC experiments are observed usually at material interfaces (discontinuities) so that the wave propagates a finite distance, and are essentially (minus interface reflections) "snap-shots" of the evolving compression

wave in a semi-infinite material. The question is at which point in the material response history does it leave an isentropic response and by how much or was the wave ever isentropic in nature? In other words, is the system dissipating energy and how is the energy being partitioned during its response history. This question is still in abeyance; however, the optimal solution would be through experimental determination (temperature and material state measurements), which are extremely difficult, but developing, or through models that describe and give the necessary wave behavior that can be subsequently tested. In this section, we introduce the Korteweg-deVries-Burgers equation and give evidence from across the drive platforms to support its further investigation.

Through the observation of acceleration profiles $\Gamma(x,t) = \partial U_p/\partial t\,|_x$ derived from the free surface or interface particle velocities $U_p(x,t)$ as a function of time t for several Lagrangian positions x, several features become apparent. But first to do this, we perform a narrow window running average ($\sim$25 points out of $\sim$5000 points total per U_p history) to reduce some of the noise in the U_p record, then take the time derivative(see Figs. 6 and 7). The first features are the bell-like structures that are best fit by $\Gamma(t) = const. + \sum_{i=1}^{N} a_i sech^2[b_i(t-t_i)]$. The $sech^2(\cdot)$ is a solution to the Korteweg-deVries (KdV) equation, suggesting that the material is responding to a similar equation. This is plausible, since the KdV equation in the past has been obtained through a set of appropriate transformations from a standard continuum description of a material with micro-structure or with relaxation[41]. We now introduce a more encompassing equation, the Korteweg-deVries-Burgers equation[42]:

$$\Gamma_t + (Q_1 + Q_2\Gamma)\Gamma_x + \beta_2\Gamma_{xx} + \beta_3\Gamma_{xxx} = 0 \qquad (3)$$

where Q_1, Q_2, β_2 and β_3 are material constants and the subscripts indicate partial derivatives. The first term gives the non-linearity, while the second and third terms are the dissipation and dispersion terms, respectively. With $\beta_2 = 0$, Eqn. 3 is the non-linear form of the KdV equation. Via Eqn. 3 we have been evaluating and characterizing experiments from the three aforementioned RWC drives and from several metals: fcc Al, bcc Ta and fcc Cu. These structures have been observed in all cases, thus far. This supports their ubiquitous nature, though it is also very interesting to understand cases in which these structures are *not* present. This is on-going work. With such a description of an averaged micro-structural response to the applied RWC impulses, our intent is to determine thermodynamic limits on the developed theoretical framework that builds constitutive models from quantum and micro-structural calculations[43].

To build confidence in this approach, we have solved the KdV equation ($\beta_2 = 0$) at one particular x_1. This is done using the inverse scattering methodology,[44, 45] where the KdV equation is transformed into the $N \times N$, time-independent Schrödinger matrix equation using $\Gamma(x_1,t)$ as the potential yielding N-eigenvalues κ for the form of $\Gamma = \Gamma_0 sech^2(\kappa x - 4\kappa^3 t)$, where the amplitude, width, and velocity of the solitary structure is related. Then this solution can be propagated in time and space to the next observed Lagrangian position x_2, yielding a good representation of the actual $\Gamma(x_2,t)$(not shown). The amplitudes and widths are not the best fit at x_2 for the propagated solution, suggesting that other mechanisms are present, like dissipation. This gives strong evidence that the KdV is characterizing the general response of the system, but the KdV needs to be modified to Eqn. 3, i.e. the inclusion of dissipation.

To investigate the dissipation character of Eqn. 3, there are several scaling arguments to be made comparing features across the three RWC drives. If Eqn. 3 is to describe the wave evolution and therefore the material response as it moves from its initial state $\mathscr{S}_0$ to its final state $\mathscr{S}_n$, then the underlying dissipation must be inherent in the limit of the wave evolution—does it give the correct entropy production as a shock. In other words, the intent is to understand if these observed structures contained within the U_p history have correct thermodynamic constraints. In terms of $U_p(t)$, Γ integrates in general to the form $u(x,t) = \delta u\, tanh(\kappa x - 4\kappa^3 t)$, where $\delta u(\kappa)$ is an infinitesimal kink-like structure. The energy that is dissipated by such a kink is given by [46]

$$E_{diss} = \nu \int_{-\infty}^{\infty} u_x^2(x,t)dx \qquad (4)$$

which yields that the $E_{diss} \propto \delta u^3$. This is similar to the well known relation that the shock state dissipates energy relative to the isentrope as $T\Delta S \approx 2\rho_0 \delta u^3\, dln[c_L(u)]/du$ to leading order, thus the infinitesimal kink-like structure is dissipating energy in a likewise manner. The constant value is $\nu =$

$[18\beta_3\rho_0/Q_2](dc_L(u)/du)_S$ when compared to the shock contribution.

Additionally, the dissipation can be investigated more directly from the experiment following Ott and Sudan[42], where the scaling of the amplitudes of these structures as a function of time or position gives a possible relationship to the underlying equation. A scaling of ΔL to the $\frac{3}{2}$ power can be shown from dimensional analysis. ΔL is the distance traveled. If the distance L is proportional to time T^α for these traveling wave structures, then from noting that $u(x,t) \propto \delta u \propto \kappa$ and that $\Gamma \propto \kappa^4$, the dimensional analysis gives $\alpha = \frac{2}{3}$. In Fig. 8, we plot this relationship between the normalized amplitudes $S = A(t)/A(0)$ as function of $(\Delta L)^{3/2}$, which indicates similarities between each of the RWC drive platforms. Also, note that the decaying amplitude is proportional to its width in the non-dissipative case[42].

In conclusion, while many valuable RWC experiments are being performed, as can be seen in this proceedings, giving invaluable information on EOS, strength, phase transition kinetics, etc., we do not want to be complacent in asking and then striving to answer difficult questions. We have presented an overview of the current developments of the FGM impactor used to generate RWC at the light-gas gun facility at LLNL, though this technology is transferrable to other platforms as well. Through a developed and now standardized manufacturing process for FGM impactors, a host of experiments are being performed mainly along elevated temperature quasi-isentropes for EOS and strength measurements focusing on tantalum, but also on aluminum (Al 1100). Other materials are also investigated to understand phase transition kinetics, like the liquid to solid transformation of water giving the first phase fraction along a quasi-isentrope. We also introduced a methodology of understanding and possibly quantifing thermodynamic constraints on material constitutive models.

But it cannot be overly emphasized that the RWC experiments still need to be determined as isentropic or characterized by the amount of dissipation, thereby informing us to its related thermodynamic material state. While such experiments (pyrometry and x-ray) are difficult in practice and will become a standard diagnostic, we must seek an alternative means of insight. Therefore, we have been working with the model KdV-Burgers equation. Since the wave structures really suggest the KdV-Burgers equation, we have seen that across the platforms a scaling in the amplitude of these structures, giving a possible link between dissipation and compression rates and material response, though a clear separation of these aspects is still open. However, such models must be tested, which mandates more experiments that determine not only the stress and density histories but temperature and phase histories of the subject material as it responds to RWC, which will further our efforts for high temperature and pressure material models.

ACKNOWLEDGMENTS

Many people have contributed to this work, especially for impactor engineering and fabrication: L. Peter Martin, Ryan T. Krone, and Tien Shen. Also, we appreciate fruitful conversations with John Klepeis and William J. Nellis. The authors gratefully acknowledge financial support for this research from the DOE. This work was performed under the auspices of the U.S. Department of Energy by the University of California Lawrence Livermore National Laboratory under contract W-7405-Eng-48.

REFERENCES

1. Nguyen, J. H., Orlikowski, D., Streitz, F. H., Moriarty, J. A., and Holmes, N. C., *J. Appl. Phys.*, **100**, 023508–023511 (2006).
2. Hall, C. A., Asay, J. R., Knudson, M. D., Stygar, W. A., Spielman, R. B., Pointon, T. D., Reisman, D. B., A., T., and Cauble, R. C., *Rev. Sci. Instr.*, **72**, 3587 (2001).
3. Edwards, J., Lorenz, K. T., Remington, B. A., Pollaine, S., Colvin, J., Braun, D., Lasinski, B. F., Reisman, D., McNaney, J. M., Greenough, J. A., Wallace, R., Louis, H., and Kalantar, D., *Phys. Rev. Let.*, **92**, 075002 (2004).
4. Harrison, E. R., *Proc. Phys. Soc.*, **84**, 213 (1964).
5. Fowler, C. M., Garn, W. B., and Caird, R. S., *J. Appl. Phys.*, **31**, 588 (1960).
6. Hawke, R. S., Duerre, D. E., Huebel, J. G., Keeler, R. N., and Klapper, H., *Phys. Earth Planet. Interiors*, **6**, 44–47 (1972).
7. Rice, M. H., McQueen, R. G., and Walsh, J. M., "Compression of Solids by Strong Shock Waves," in *Solid State Physics: Advances in Research and*

Applications, edited by F. Seitz and D. Turnbull, Academic Press, 1958, vol. 6, pp. 1–60.
8. Asay, J. R., *Int. J. Impact Engng.*, **20**, 27–61 (1997).
9. Barker, L. M., "High-Pressure Quasi-isentropic Impact Experiments," in *Shock Waves in Condensed Matter-1983*, edited by J. R. Asay, R. A. Graham, and G. K. Straub, Elsevier Science, 1984, p. 217.
10. Chhabildas, L. C., and Barker, L. M., Dynamic quasi-isentropic compression techniques: applications to aluminum and tungsten, Tech. Rep. SAND86-1888, Sandia National Laboratories (1986).
11. Barker, L. M., and Hollenbach, R. E., *J. Appl. Phys.*, **41**, 4208 (1970).
12. Weir, S. T., Mitchell, A. C., and Nellis, W. J., *Phys. Rev. Let.*, **76**, 1860–1863 (1996).
13. Smith, R. F., Eggert, J. H., Jankowski, A., Celliers, P. M., Edwards, M. J., Gupta, Y. M., Asay, J. R., and Collins, G. W., *Phys. Rev. Let.*, **98**, 065701 (2007).
14. Davis, J.-P., *J. Appl. Phys.*, **99**, 103512 (2006).
15. Lee, G. W., Evans, W. J., and Yoo, C.-S., *Phys. Rev. B*, **74**, 134112 (2006).
16. Partouche-Sebban, D., Pelissier, J. L., Abeyta, F. G., Anderson, W. W., Byers, M. E., Dennis-Koller, D., Esparza, J. S., Hixson, R. S., Holtkamp, D. B., Jensen, B. J., King, J. C., Rigg, P. A., Rodriguez, P., Shampine, D. L., Stone, J. B., Westley, D. T., Borror, S. D., and Kruschwitz, C. A., *Journal of Applied Physics*, **97**, 043521 (2005).
17. Kalantar, D. H., Belak, J. F., Collins, G. W., Colvin, J. D., Davies, H. M., Eggert, J. H., Germann, T. C., Hawreliak, J., Holian, B. L., Kadau, K., Lomdahl, P. S., Lorenzana, H. E., Meyers, M. A., Rosolankova, K., Schneider, M. S., Sheppard, J., Stolken, J. S., and Wark, J. S., *Physical Review Letters*, **95**, 075502 (2005).
18. Strand, O. T., Goosman, D. R., Martinez, C., Whitworth, T. L., and Kuhlow, W. W., *Rev. Sci. Instr.*, **77**, 083108 (2006).
19. Martin, L. P., Orlikowski, D., and Nguyen, J. H., *Mat. Sci. Eng. A*, **427**, 83–91 (2006).
20. Martin, L. P., Patterson, J. R., Orlikowski, D., and Nguyen, J. H., *accepted J. Appl. Phys.* (2007).
21. Krone, R. T., Martin, L. P., Patterson, J. R., Orlikowski, D., and Nguyen, J. H., *accepted Mat. Sci. Eng. A* (2007).
22. Barker, L. M., and Hollenbach, R. E., *J. Appl. Phys.*, **43**, 4669 (1972).
23. Fowles, R., and Williams, R. F., *J. Appl. Phys.*, **41**, 360 (1970).
24. Seaman, L., *J. Appl. Phys.*, **45**, 4303 (1974).
25. Aidun, J. B., and Gupta, Y. M., *J. Appl. Phys.*, **69**, 6998 (1991).
26. Hayes, D., Backward integration of the equations of motion to correct for free surface perturbations, Tech. Rep. SAND2001-1440, Sandia National Lab. (2001).
27. Reisman, D. B., Toor, A., Cauble, R. C., Hall, C. A., Asay, J. R., Knudson, M. D., and Furnish, M. D., *J. Appl. Phys.*, **89**, 1625 (2001).
28. Wallace, D. C., *Phys. Rev. B*, **22**, 1477 (1980).
29. Wallace, D. C., *Phys. Rev. B*, **22**, 1487 (1980).
30. Wallace, D. C., *Phys. Rev. B*, **22**, 1495 (1980).
31. Huang, H., and Asay, J. R., *J. Appl. Phys.*, **100**, 043514 (2006).
32. Huang, H., and Asay, J. R., *J. Appl. Phys.*, **101**, 063550 (2007).
33. Avrami, M., *J. Chem. Phys.*, **7**, 1103–1112 (1939).
34. Avrami, M., *J. Chem. Phys.*, **8**, 212–224 (1940).
35. Avrami, M., *J. Chem. Phys.*, **9**, 177–184 (1941).
36. Drolet, F., Elder, K. R., Grant, M., and Kosterlitz, J. M., *Phys. Rev. E*, **61**, 6705 (2000).
37. Florando, J., Lassila, D., and et al., Plasticity at high pressures and strain rates using oblique-impact isentropic-compression experiments, private communication.
38. Jarmakani, H., McNaney, J. M., Kad, B., Orlikowski, D., Nguyen, J. H., and Meyers, M. A., *Mat. Sci. Eng. A*, p. doi:10.1016/j.msea.2006.09.118 (2007).
39. Bastea, M., and et al., *to be published* (2007).
40. Nguyen, J. H., and et al., *to be published* (2007).
41. Engelbrecht, J., *Nonlinear Wave Processes of Deformation of Solids*, vol. 16 of *Mono. and studies in mathe.*, Pitman Advanced Pub., 1983.
42. Ott, E., and Sudan, R. N., *Phys. Fluids*, **13**, 1432 (1970).
43. Moriarty, J. A., Benedict, L. X., Glosli, J. N., Hood, R. Q., Orlikowski, D., Patel, M. V., Söderlind, P., Streitz, F. H., Tang, M., and Yang, L. H., *J. Mat. Res.*, **21**, 563 (2006).
44. Hirota, R., *Phys. Rev. Let.*, **27**, 1192 (1971).
45. Gardner, C. S., Greene, J. M., Kruskal, M. D., and Miura, R. M., *Comm. Pure Appl. Mathe.*, **27**, 97 (1974).
46. Falkovich, G., and Fouxon, A., *New J. Phys.*, **6**, 50 (2004).